JP Journal of Heat and Mass Transfer

http://www.pphmj.com
http://dx.doi.org/10.17654/HM014030289
Volume 14, Number 3, 2017, Pages 289-316 **ISSN: 0973-5763**

INFLUENCE OF INTERNAL HEAT GENERATION AND THERMAL RADIATION ON THE MHD-FREE CONVECTION OF NON-NEWTONIAN FLUIDS OVER A VERTICAL PERMEABLE PLATE IN POROUS MEDIA WITH SORET/DUFOUR EFFECTS

Chuo-Jeng Huang

Department of Aircraft Engineering
Air Force Institute of Technology
Taiwan (R. O. C.)

Abstract

An analysis is presented to investigate the influence of internal heat generation and thermal radiation on the MHD-free convection of non-Newtonian fluids over a vertical permeable plate in porous media. The heat and mass transfer characteristics due to the effect of uniform blowing/suction and double-diffusive are numerically analyzed. The surface of the vertical plate has a uniform wall temperature and a uniform wall concentration (UWT/UWC). Non-similar solutions for the transformed governing equations by Keller box method are obtained. Comparisons showed excellent agreements with the numerical data in previous works. Numerical data for the dimensionless temperature profile, the dimensionless concentration profile, the local Nusselt number and the local Sherwood number are presented for the main parameters: the power-law index of the non-

Received: December 18, 2016; Accepted: March 20, 2017

Keywords and phrases: internal heat generation, thermal radiation, non-Newtonian fluid, MHD-free convection, vertical permeable plate, porous media.

Newtonian fluid, the blowing/suction parameter, the magnetic field parameter, the internal heat generation coefficient and the thermal radiation parameter which are entered in tables or plotted in figures.

1. Introduction

The boundary-layer flow of coupled heat and mass transfer (or double-diffusion) in porous medium has gained a considerable attention of many researchers in recent years. This is justified reason by the point that porous media play a vital role in many engineering and geophysical applications such as thermal insulation of buildings, nuclear reactor cooling system, nuclear waste disposals, energy recovery of petroleum resources, chemical reactors, extraction of geothermal energy, filtration processes, etc. Nield and Bejan [1], recently, presented a comprehensive account of the available information in the field.

The Soret effect referred to species differentiation developing in an initial homogeneous mixture submitted to a thermal gradient. The Dufour effect referred to heat flux produced by a concentration gradient. Anghel et al. [2] examined the Dufour and Soret effects on free convection boundary-layer flow over a vertical surface embedded in a porous medium. Cheng [3] presented the double diffusion from a vertical wavy surface in a porous medium saturated with a non-Newtonian fluid. Postelnicu [4] studied the heat and mass transfer by natural convection at a stagnation point in a porous medium considering Soret and Dufour effects. Cheng [5] investigated the Soret and Dufour effects on free convection heat and mass transfer from an arbitrarily inclined plate in a porous medium with constant wall temperature and concentration.

A number of industrially important fluids including fossil fuels exhibit non-Newtonian fluid behavior. Non-Newtonian power law fluids are so widespread in industrial processes and in the environment that it would be no exaggeration to affirm that Newtonian shear flows are the exception rather than the rule. Shenoy [6] presented many interesting applications of non-Newtonian power law fluids with yield stress on convective heat transport in fluid saturated porous media considering geothermal and oil reservoir

engineering applications. Chen and Chen [7] presented similarity solutions for natural convection of a non-Newtonian fluid over vertical surfaces in porous media. Gorla and Kumari [8] studied nonsimilar solutions for free convection in non-Newtonian fluids along a vertical plate in a porous medium. Cheng [9] studied the natural convection heat and mass transfer of non-Newtonian power law fluids with yield stress in porous media from a vertical plate with variable wall heat and mass fluxes. Mahdy and Hady [10] reported the effect of thermophoretic particle deposition in non-Newtonian free convection flow over a vertical plate with magnetic field effect.

Considerable of physical phenomena involved free convection driven by internal heat generation. The most important applications are in the reactor safety analyses, metal waste form development for spent nuclear fuel, fire and combustion studies, and radioactive materials storage. A new class of similarity solutions was obtained for an isothermal vertical plate in a semi-infinite quiescent fluid with internal heat generation decaying exponentially by Crepeau and Clarksean [11]. Postelnicu and Pop [12] then used the model developed by Crepeau and Clarksean [11] to study the similarity solutions of free convection boundary layers over vertical and horizontal surfaces in porous media with internal heat generation. Grosan and Pop [13] reported the free convection boundary layer developed by a vertical flat plate in porous medium, saturated with a non-Newtonian fluid with internal heat generation. Mohamed [14] analyzed the effect of lateral mass flux on the natural convection boundary layers induced by a heated vertical plate embedded in a saturated porous medium with internal heat generation. Mahmoud [15] described the radiation effect on free convection of a non-Newtonian fluid over a vertical cone embedded in a porous medium with heat generation. Yih and Huang [16] extended the research of Grosan and Pop [13] to report the effect of internal heat generation on free convection heat and mass transfer of non-Newtonian fluids flow over a vertical plate in porous media with variable wall temperature and concentration.

In many new engineering areas, processes such as energy processes of fossil fuel combustion, solar power technology, astrophysical flows, gas turbines and the various propulsion devices for aircraft, missiles, satellites,

and space vehicle re-entry occur at high temperatures so knowledge of radiation heat transfer beside the convective heat transfer plays a very important role and hence its effect cannot be neglected. Also, thermal radiation is of major importance in many processes in engineering areas which occur at a very high temperature for the design of many advanced energy conversion systems and pertinent equipment. The Rosseland approximation is used to describe the radiative heat flux in the energy equation. Raptis [17] described the radiation and free convection flow through a porous medium. Mohammadien and El-Amin [18] considered the thermal dispersion-radiation effects on non-Darcy natural convection in a fluid saturated porous medium. El-Hakiem and El-Amin [19] investigated thermal radiation effect on non-Darcy natural convection with lateral mass transfer. Seddeek [20] examined the thermal radiation and buoyancy effects on MHD free convective heat generating flow over an accelerating permeable surface with temperature-dependent viscosity. Tai and Char [21] examined the Soret and Dufour effects on free convection flow of non-Newtonian fluids along a vertical plate embedded in a porous medium with thermal radiation. Sheikholeslami et al. [22] presented the effect of thermal radiation on magnetohydrodynamics nanofluid flow and heat transfer by means of two phase model.

Magnetohydrodynamic (MHD) boundary layer flow for an electrically conducting fluid in porous medium is of considerable interest in geothermal system, geophysical engineering, aerodynamic processes, underground disposal of nuclear waste materials and many others. Because of the wide application of the characteristic of the MHD in porous medium, it becomes one of the major topics of research in the last two centuries. Cheng [23] examined the effect of magnetic field on heat and mass transfer by natural convection from vertical surfaces in porous media - an integral approach. Postelnicu [24] studied the influence of a magnetic field on heat and mass transfer by natural convection from vertical surfaces in porous media considering Soret and Dufour effects. Cheng [25] used an integral approach for hydromagnetic natural convection heat and mass transfer from vertical surfaces with power-law variation in wall temperature and concentration in

porous media. Partha et al. [26] accounted for the Soret and Dufour effects in a non-Darcy porous medium. Bakier and Mansour [27] considered the combination of magnetic field and thermophoresis particle deposition in free convection boundary layer from a vertical flat plate embedded in a porous medium. Rashad [28] examined the influence of radiation on MHD free convection from a vertical flat plate embedded in porous media with thermophoretic deposition of particles. Chamkha and Ben-Nakhi [29] studied the MHD mixed convection-radiation interaction along a permeable surface immersed in a porous medium in the presence of Soret and Dufour's effects. Mahdy et al. [30] investigated the double-diffusive convection with variable viscosity from a vertical truncated cone in porous media in the presence of magnetic field and radiation effects. Prasad et al. [31] studied the thermo-diffusion and diffusion-thermo effects on MHD free convection flow past a vertical porous plate embedded in a non-Darcian porous medium. Hsiao et al. [32] analyzed the influence of thermophoretic particle deposition on MHD free convection flow of non-Newtonian fluids from a vertical plate embedded in porous media considering Soret and Dufour effects.

In the above paper, many authors have studied the effects of magnetic field in porous media over mixed, natural and force convection heat and mass transfer problems. Therefore, current work is to extend the work of Tai and Char [21] and Postelnicu [24] by investigating the internal heat generation and thermal radiation on the MHD-free convection of non-Newtonian fluids over a vertical permeable plate in porous media with Soret/Dufour effects.

2. Formulation and Analysis

The considered problem is the effect of internal heat generation and thermal radiation on steady MHD-free convective flow and mass transfer of a uniform blowing/suction and non-Newtonian fluids over a vertical plate in porous media with Soret/Dufour effects and where the boundary condition is uniform wall temperature T_w and uniform wall concentration C_w (UWT/UWC), respectively. Consider a two-dimensional, steady, laminar

flow of an incompressible electrically conducting fluid over a flat plate in the presence of a transverse magnetic field B_0, as shown in Figure 1, while the induced magnetic field due to the motion of the electrically conducting fluid is negligible. The origin of the coordinate system is the leading edge of the vertical flat plate, where x and y are Cartesian coordinates for the distance along and normal to, respectively, the vertical flat plate surface.

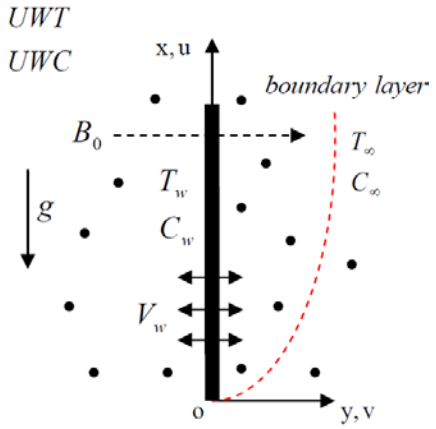

Figure 1. The flow model and the physical coordinate system.

All the fluid properties are assumed to be constant except for the density variation in the buoyancy term. Introducing the boundary layer and Boussinesq approximations, the governing equations and the boundary conditions based on the Darcy law can be written as follows:

Continuity equation:

$$\frac{\partial u}{\partial x} + \frac{\partial v}{\partial y} = 0. \tag{1}$$

Momentum (Darcy) equation:

$$u^n + \frac{K(n)\cdot \sigma \cdot B_0^2}{\mu}\cdot u = -\frac{K(n)}{\mu}\left(\frac{\partial p}{\partial x} + \rho g\right), \tag{2}$$

$$v^n = -\frac{K(n)}{\mu}\left(\frac{\partial p}{\partial y}\right). \tag{3}$$

Energy equation:

$$u\frac{\partial T}{\partial x}+v\frac{\partial T}{\partial y}=\alpha_m\frac{\partial^2 T}{\partial y^2}+\frac{D_m}{C_s}\cdot\frac{k_T}{C_p}\cdot\frac{\partial^2 C}{\partial y^2}+\frac{q'''}{\rho_\infty\cdot C_p}-\frac{\alpha}{k}\frac{\partial q_r}{\partial y}. \tag{4}$$

Concentration equation:

$$u\frac{\partial C}{\partial x}+v\frac{\partial C}{\partial y}=D_m\frac{\partial^2 C}{\partial y^2}+\frac{D_m\cdot k_T}{T_m}\cdot\frac{\partial^2 T}{\partial y^2}. \tag{5}$$

Radiation equation (Rosseland diffusion approximation):

$$q_r=-\frac{4\sigma_0}{3\chi}\frac{\partial T^4}{\partial y}. \tag{6}$$

Boussinesq approximation:

$$\rho=\rho_\infty[1-\beta_T(T-T_\infty)-\beta_C(C-C_\infty)]. \tag{7}$$

Boundary conditions:

$$y=0: v=V_w,\ T=T_w,\ C=C_w, \tag{8}$$

$$y\to\infty: u=0,\ T=T_\infty,\ C=C_\infty. \tag{9}$$

Here, u and v are the Darcian velocities in the x- and y-directions, respectively; n is the power-law index of the non-Newtonian fluid; $K(n)$ is the permeability of the porous medium; σ is the electric conductivity of the fluid; B_0 is the externally imposed magnetic field in the y-direction; g is the acceleration due to gravity; p, ρ and μ are the pressure, the density and the absolute viscosity, respectively; T and C are the volume-averaged temperature and concentration, respectively; α_m and D_m are the equivalent thermal diffusivity and mass diffusivity, respectively; C_p and C_s are the specific heat at constant pressure and concentration susceptibility; k_T is the thermal diffusion ratio; T_m is the mean fluid temperature; q^m is the internal heat generation rate per unit volume; q_r is radiative heat flux; σ_0 is the Stefan-Boltzmann constant; χ is the mean absorption coefficient; β_T and β_C

are the thermal and concentration expansion coefficients of the fluid, respectively; and V_w is the uniform blowing/suction velocity.

The power-law fluid index n for various fluids is as follows:

(i) $n < 1$ for pseudo-plastic fluids (for example, the polymer solution) or shear-thinning fluids that have a lower apparent viscosity at higher shear rates.

(ii) $n = 1$ for Newtonian fluids (for instance, air and water) where the shear stress is directly proportional to the shear rate.

(iii) $n > 1$ for dilatant fluids (for example, the suspensions of sand) or shear-thickening fluids for which there is an increase in the apparent viscosity at higher shear rates.

For the power law model of Ostwald-de-Waele, Christopher and Middleman [33] and Dharmadhirkari and Kale [34] proposed the following relationships for the permeability:

$$K(n) = \begin{cases} \dfrac{6}{25}\left(\dfrac{n\varepsilon}{3n+1}\right)^{n}\left[\dfrac{\varepsilon d}{3(1-\varepsilon)}\right]^{n+1}, & [33] \\ \dfrac{2}{\varepsilon}\left[\dfrac{d\varepsilon^{2}}{8(1-\varepsilon)}\right]^{n+1}\left(\dfrac{6n+1}{10n-3}\right)\left(\dfrac{16}{75}\right)^{\frac{3(10n-3)}{(10n+11)}}, & [34] \end{cases} \tag{10}$$

where d is the particle diameter while ε is the porosity.

The stream function ψ is defined by

$$u = \partial\psi/\partial y \text{ and } v = -\partial\psi/\partial x. \tag{11}$$

Therefore, the continuity equation is automatically satisfied.

Next, consider the governing equations (2) and (3). Cross-differentiation $\partial(u^n)/\partial y - \partial(v^n)/\partial x$ eliminates the pressure terms in equations (2) and (3). Further, by using the boundary layer approximation $(\partial/\partial x << \partial/\partial y,$ $v << u)$, it yields

$$\frac{\partial u^n}{\partial y} + \left(\frac{K(n) \cdot \sigma \cdot B_0^2}{\mu} \right) \frac{\partial u}{\partial y} = \frac{\rho_\infty \cdot g \cdot K(n)}{\mu} \left(\beta_T \frac{\partial T}{\partial y} + \beta_C \frac{\partial C}{\partial y} \right). \quad (12)$$

Integrating equation (12) once and with the aid of equation (9) yields

$$u^n + \left(\frac{K(n) \cdot \sigma \cdot B_0^2}{\mu} \right) \cdot u = \frac{\rho_\infty \cdot g \cdot K(n)}{\mu} [\beta_T (T - T_\infty) + \beta_C (C - C_\infty)]. \quad (13)$$

The second, third and fourth terms on the right-hand side of the energy equation (4) represent the Dufour effect, the heat generation rate per unit volume and the thermal radiation heat flux, and the last term of concentration equation (5) denotes the Soret effect. Note that, in equation (6), the Rosseland diffusion approximation is used to describe the radiative heat flux [17-22]. Further, assume that the temperature differences within the flow are sufficiently small so that T^4 in equation (6) can be expanded in Taylor series about T_∞, and discard higher-order terms in the usual manner. Thus,

$$T^4 \cong 4T_\infty^3 T - 3T_\infty^4. \quad (14)$$

The following dimensionless variables are invoked:

$$\xi = \frac{2V_w x}{\alpha Ra_x^{1/2n}}, \quad (15.1)$$

$$\eta = \frac{y}{x} Ra_x^{1/2n}, \quad (15.2)$$

$$f(\xi, \eta) = \frac{\psi}{\alpha Ra_x^{1/2n}}, \quad (15.3)$$

$$\theta(\xi, \eta) = \frac{T - T_\infty}{T_w - T_\infty}, \quad (15.4)$$

$$\phi(\xi, \eta) = \frac{C - C_\infty}{C_w - C_\infty}, \quad (15.5)$$

$$Ra_x = \frac{\rho_\infty g \beta_T [T_w - T_\infty] K(n)}{\mu} \left(\frac{x}{\alpha} \right)^n, \quad (15.6)$$

where Ra_x is the local Rayleigh number.

Following Mohamed [14], the internal heat generation rate per unit volume q''' is modeled according to the following equation:

$$q''' = A^* \frac{k[T_w(x) - T_\infty]}{x^2} Ra_x^{1/n} e^{-\eta}, \tag{16}$$

where k is the equivalent thermal conductivity of the porous medium, and A^* is the internal heat generation coefficient. Notably, $A^* = 0$ corresponds to case 1 without internal heat generation (designated as NIHG), and $A^* > 0$ corresponds to case 2 with internal heat generation (WIHG).

Substituting equations (14)-(16) into equations (13), (4)-(6), (8)-(9), we obtain

$$(f')^n + M \cdot f' = \theta + N \cdot \phi, \tag{17}$$

$$\left(1 + \frac{4}{3} R_d\right)\theta'' + \frac{1}{2} f\theta' + D\phi'' + A^* e^{-\eta} = \frac{1}{2}\xi\left(f' \frac{\partial\theta}{\partial\xi} - \theta' \frac{\partial f}{\partial\xi}\right), \tag{18}$$

$$\frac{1}{Le}\phi'' + \frac{1}{2} f\phi' + S\theta'' = \frac{1}{2}\xi\left(f' \frac{\partial\phi}{\partial\xi} - \phi' \frac{\partial f}{\partial\xi}\right). \tag{19}$$

The boundary conditions are defined as follows:

$$\eta = 0 : f = -\frac{\xi}{2}, \ \theta = 1, \ \phi = 1, \tag{20}$$

$$\eta \to \infty : \theta = 0, \ \phi = 0. \tag{21}$$

For the new variables, the Darcian velocities in the x- and y-directions are also, respectively, obtained by

$$u = \frac{\alpha Ra_x^{1/n}}{x} f', \tag{22}$$

$$v = -\frac{\alpha Ra_x^{1/2n}}{2x}\left[f + \xi \frac{\partial f}{\partial\xi} - \eta f'\right], \tag{23}$$

where M is the magnetic parameter defined as

$$M = \left(\frac{K(n)\cdot\sigma\cdot B_0^2}{\mu}\right)\cdot\left(\frac{\rho_\infty\cdot g\cdot\beta_T(T_w-T_\infty)\cdot K(n)}{\mu}\right)^{\frac{1-n}{n}}, \tag{24}$$

where primes denote differentiation with respect to $\eta\cdot\xi$ defined in equation (15.1) is the surface blowing/suction parameter; equation (20) can be obtained by integrating equation (23) versus ξ once and by setting $\eta = 0$ (at the surface, $y = 0$, then $\eta = 0$), and with the help of boundary equation (8). On one hand, for the case of blowing, $V_w > 0$ and hence $\xi > 0$. On the other hand, for the case of suction, $V_w < 0$ and hence $\xi < 0$. Besides, the buoyancy ratio N, the Lewis number Le, the Dufour parameter D and the Soret parameter S are, respectively, defined as follows:

$$N = \frac{\beta_C[C_w - C_\infty]}{\beta_T[T_w - T_\infty]}, \quad Le = \frac{\alpha_m}{D_m}, \tag{25}$$

$$D = \frac{D_m\cdot k_T\cdot[C_w - C_\infty]}{C_s\cdot C_P\cdot\alpha_m\cdot[T_w - T_\infty]}, \quad S = \frac{D_m\cdot k_T\cdot[T_w - T_\infty]}{T_m\cdot[C_w - C_\infty]}, \tag{26}$$

$$R_d = \frac{4\sigma_0 T_\infty^3}{k\chi}. \tag{27}$$

The results for heat and mass transfer rates have practical applications. The heat and mass transfer rates are expressed in terms of the local Nusselt number Nu_x and the local Sherwood number Sh_x, which are, respectively, defined as follows:

$$Nu_x = \frac{h_x x}{k} = \frac{q_w x}{[T_w - T_\infty]k_T} = \frac{\left[-k\left(\frac{\partial T}{\partial y}\right)\Big|_{y=0} + q_r\right]x}{[T_w - T_\infty]k_T}, \tag{28}$$

$$Sh_x = \frac{h_{m,x} x}{D_m} = \frac{m_w x}{[C_w - C_\infty]D_m} = \frac{-\left(\frac{\partial C}{\partial y}\right)\Big|_{y=0} x}{[C_w - C_\infty]D_m}. \tag{29}$$

By applying equations (6), (14)-(15), the local Nusselt number Nu_x and the local Sherwood number Sh_x in terms of $Ra_x^{1/2n}$ are, respectively, obtained by

$$\frac{Nu_x}{Ra_x^{1/2n}} = -\left(1 + \frac{4R_d}{3}\right)\theta'(\xi, 0), \tag{30}$$

$$\frac{Sh_x}{Ra_x^{1/2n}} = -\phi'(\xi, 0). \tag{31}$$

It may be noticed that for $A^* = 0$ (without internal heat generation effect), $M = 0$ (without magnetic field effect), $\xi = 0$ (without blowing/ suction effect), equations (17)-(21) are reduced to those of Tai and Char [21] where a similar solution was obtained previously.

3. Numerical Method and Validation

The present analysis integrates the system of equations (17)-(21) by the implicit finite difference approximation together with the modified Keller box method of Cebeci and Bradshaw [35]. First of all, the partial differential equations converted into a system of five first-order equations. These first-order equations are then expressed in finite difference forms and solved along with their boundary conditions by applying an iterative scheme. This approach improves the convergence rate and the computation times.

Computations were performed with a personal computer with $\Delta\xi = 0.1$ and the first step size $\Delta\eta_l = 0.01$. The variable grid parameter is chosen 1.01 and the value of $\eta_\infty = 30$. The iterative procedure is stopped to give the final temperature and concentration distributions when the error in computing the θ'_w and ϕ'_w in the next procedure becomes less than 10^{-5}.

4. Results and Discussion

To validate the numerical method used, the heat and mass transfer results

of the present results are compared to those of previously published papers. The accuracy of this method was verified by comparing the results with those of Yih and Huang [16], Tai and Char [21], Postelnicu [24], Chamkha and Ben-Nakhi [29] and Hsiao et al. [32]. Table 1 lists the comparison of present results for various values of ξ with $N = D = S = M = R_d = A^* = 0$, $n = 1$. Table 2 lists the comparison of present results for various values of M, D and S with $\xi = R_d = A^* = 0$, $n = Le = 1$. Table 3 lists the comparison of present results for various values of n, R_d, D, S, N and Le with $\xi = M = A^* = 0$. Table 4 lists the comparison of $-\theta'(\xi, 0)$ and $-\phi'(\xi, 0)$ for various values of A^* and n with $D = S = R_d = \xi = M = 0$, $N = 4$, $Le = 10$. All the values in Tables 1 to 4 list the comparisons showed excellent agreement with the numerical data in previous works.

Table 1. Comparison of present results for various values of ξ with $N = D = S = M = R_d = A^* = 0$, $n = 1$

	$-\theta'(\xi, 0)$	
ξ	Chamkha and Ben-Nakhi [29]	Present results
–4	1.9989	2.0014
–2	1.0726	1.0725
0	0.4440	0.4437
2	0.1424	0.1407
4	0.0340	0.0329

Table 2. Comparison of present results for various values of M, N, D and S with $\xi = R_d = A^* = 0$, $n = Le = 1$

				$-\theta'(\xi, 0)$			$-\phi'(\xi, 0)$		
M	N	D	S	Postelnicu [24]	Hsiao et al. [32]	Present results	Postelnicu [24]	Hsiao et al. [32]	Present results
0	0.5	0.075	0.8	0.5550	0.5550	0.5550	0.2876	0.2876	0.2876
1	0.5	0.075	0.8	0.3925	0.3925	0.3925	0.2033	0.2033	0.2034
0	1	0.03	2.0	0.7144	0.7144	0.7144	-0.1359	-0.1395	-0.1395
1	1	0.03	2.0	0.5051	0.5051	0.5051	-0.0986	-0.0986	-0.0986

Table 3. Comparison of $-\theta'(\xi, 0)$ and $-\phi'(\xi, 0)$ for various values of n, R_d, D, S, N and Le with $\xi = M = A^* = 0$

n	R_d	D	S	N	Le	$-\theta'(\xi, 0)$		$-\phi'(\xi, 0)$	
						Tai and Char [21]	Present results	Tai and Char [21]	Present results
0.5	1.25	0.03	0.4	0.5	4	0.7476	0.7471	1.2420	1.2483
0.8	1.25	0.03	0.4	0.5	4	0.7692	0.7687	1.1355	1.1381
1.0	1.25	0.03	0.4	0.5	4	0.7832	0.7828	1.1053	1.1062
1.5	1.25	0.03	0.4	0.5	4	0.8091	0.8090	1.0675	1.0677
2.5	1.25	0.03	0.4	0.5	4	0.8380	0.8376	1.0411	1.0406
1.5	0	0.15	0.1	0.2	2	0.4372	0.4372	0.7222	0.7222
1.5	0.25	0.15	0.1	0.2	2	0.5063	0.5063	0.7403	0.7403
1.5	1.25	0.15	0.1	0.2	2	0.7235	0.7235	0.7726	0.7724
1.5	5	0.15	0.1	0.2	2	1.2505	1.2518	0.8000	0.8002

Table 4. Comparison of $-\theta'(\xi, 0)$ and $-\phi'(\xi, 0)$ for various values of A^* and n with $D = S = R_d = \xi = M = 0$, $N = 4$, $Le = 10$

A^*	n	$-\theta'(\xi, 0)$		$-\phi'(\xi, 0)$	
		Yih and Huang [16]	Present results	Yih and Huang [16]	Present results
0	0.5	1.0105	1.0104	6.3671	6.3671
0	1.0	0.6811	0.6810	3.2892	3.2892
0	2.0	0.6030	0.6029	2.4022	2.4022
1	0.5	0.2404	0.2402	6.4412	6.4412
1	1.0	-0.0191	-0.0191	3.3311	3.3311
1	2.0	-0.0837	-0.0837	2.4247	2.4247

In this investigation, the problem of effect of internal heat generation and thermal radiation coupled heat and mass transfer by MHD-free convection of a non-Newtonian fluid flow along a vertical permeable plate in the presence of Soret/Dufour effects has been studied. Representative numerical results for the dimensionless temperature and concentration profiles and the local Nusselt and Sherwood numbers with the buoyancy ratio $N = 2$, the Lewis number $Le = 1$, the Dufour parameter $D = 0.2$, the Soret parameter

$S = 0.1$, internal heat generation A^* ranging from 0 to 1, the thermal radiation parameter R_d ranging from 0 to 10, the magnetic field parameter M ranging from 0 to 4, the non-Newtonian fluid n ranging from 0.5 to 2.0, and the blowing/suction parameter ξ ranging from -2 to 2 are shown in Figures 2-6.

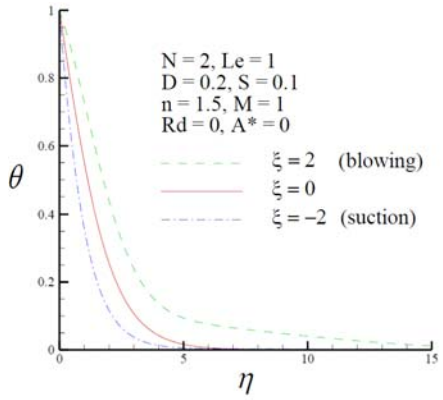

(a)

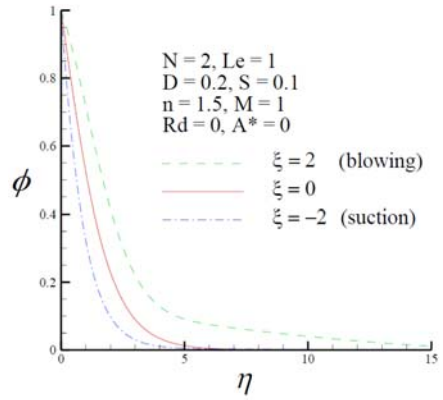

(b)

Figure 2. (a) The dimensionless temperature profile and (b) the dimensionless concentration profile for three values of the blowing/suction parameter ξ.

Figure 2 portrays the dimensionless temperature and concentration profiles for three values of the blowing/suction parameter ξ ($\xi = -2$, 0 and 2) with $N = 2$, $Le = 1$, $D = 0.2$, $S = 0.1$, $n = 1.5$, $M = 1$, $R_d = 0$, $A^* = 0$, respectively. These two figures show that the dimensionless temperature and concentration profiles decrease monotonically from the surface of the vertical flat plate to the ambient. Both the thermal boundary layer thickness δ_T and the concentration boundary layer thickness δ_C decrease for the case of suction. However, this trend reversed for the case of blowing. For suction case, it decreases the dimensionless temperature profiles θ and the dimensionless concentration profiles ϕ; thus increases the dimensionless surface temperature gradient $-\theta'(\xi, 0)$ and the dimensionless surface concentration gradient $-\phi'(\xi, 0)$. The analysis has shown that the dimensionless temperature and concentration profiles are appreciably influenced by blowing/suction parameter.

Table 5. The values of $Nu_x/Ra_x^{1/2n}$ and $Sh_x/Ra_x^{1/2n}$ for various values of ξ with $N = 2$, $Le = 1$, $D = 0.2$, $S = 0.1$, $n = 1.5$, $M = 1$, $R_d = 0$, $A^* = 0$

ξ	$Nu_x/Ra_x^{1/2n}$	$Sh_x/Ra_x^{1/2n}$
–2	0.9620	1.0678
–1	0.6971	0.7626
0	0.4868	0.5214
1	0.3270	0.3409
2	0.2092	0.2111

Table 5 lists the values of local Nusselt number $Nu_x/Ra_x^{1/2n}$ and the local Sherwood number $Sh_x/Ra_x^{1/2n}$ for various values of ξ with $N = 2$, $Le = 1$, $D = 0.2$, $S = 0.1$, $n = 1.5$, $M = 1$, $R_d = 0$ and $A^* = 0$. In general, it has been found that both the local Nusselt number and the local Sherwood number increase owing to the case of suction, i.e., $\xi < 0$. This is because for the case of suction increases both the dimensionless surface

temperature and concentration gradients, as shown in Figure 2. With the aid of equations (30)-(31), the larger the dimensionless surface temperature and concentration gradients, the greater the local Nusselt and Sherwood numbers.

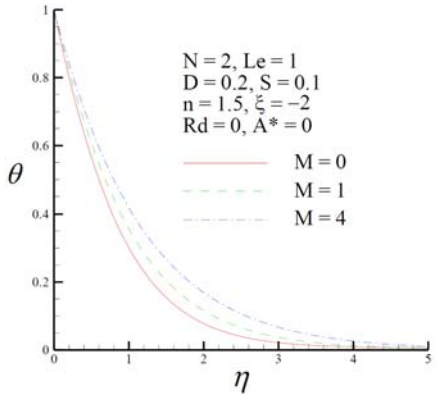

(a)

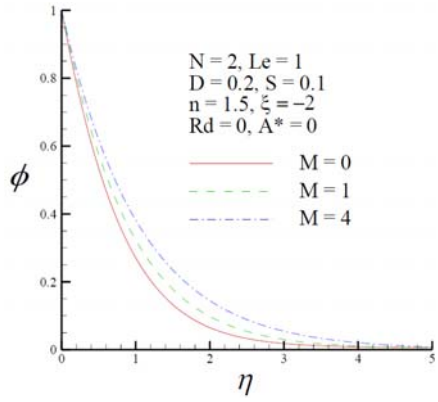

(b)

Figure 3. (a) The dimensionless temperature profile and (b) the dimensionless concentration profile for three values of magnetic field parameter *M*.

The effect of the magnetic field parameter M $(M = 0, 1 \text{ and } 4)$ on the dimensionless temperature profile and the dimensionless concentration profile with $N = 2$, $Le = 1$, $D = 0.2$, $S = 0.1$, $n = 1.5$, $\xi = -2$, $R_d = 0$

and $A^* = 0$ is plotted in Figure 3, respectively. Inspecting of this figure shows that the dimensionless temperature profile and the dimensionless concentration profile decreases monotonically as the distance η from the plate increases. It is also observed that the increase of the magnetic field parameter M leads to a tendency to decrease the flow velocity; thus, reducing both the dimensionless wall temperature gradient $-\theta'(\xi, 0)$ and the dimensionless wall concentration gradient $-\phi'(\xi, 0)$. This fact can also be demonstrated from the second term on the left-hand side in equation (17). The analysis has shown that the dimensionless temperature and concentration profiles are significantly influenced by magnetic field parameter.

Table 6. The values of $Nu_x/Ra_x^{1/2n}$ and $Sh_x/Ra_x^{1/2n}$ for various values of M with $N = 2$, $Le = 1$, $D = 0.2$, $S = 0.1$, $n = 1.5$, $\xi = -2$, $R_d = 0$ and $A^* = 0$

M	$Nu_x/Ra_x^{1/2n}$	$Sh_x/Ra_x^{1/2n}$
0.0	1.0717	1.1812
0.5	1.0078	1.1151
1.0	0.9620	1.0678
1.5	0.9286	1.0332
2.0	0.9040	1.0080

Table 6 lists the values of local Nusselt number $Nu_x/Ra_x^{1/2n}$ and the local Sherwood number $Sh_x/Ra_x^{1/2n}$ for various values of the magnetic field parameter M with $N = 2$, $Le = 1$, $D = 0.2$, $S = 0.1$, $n = 1.5$, $\xi = -2$, $R_d = 0$ and $A^* = 0$. Generally, it has been observed that enhancing the magnetic field parameter M reduces both the local Nusselt number and the local Sherwood number. This is due to the fact that enhancing the magnetic field parameter M tends to decreases the dimensionless surface temperature gradients and the dimensionless surface concentration gradients, as shown in Figure 3, thus lowering the local Nusselt number and the local Sherwood number.

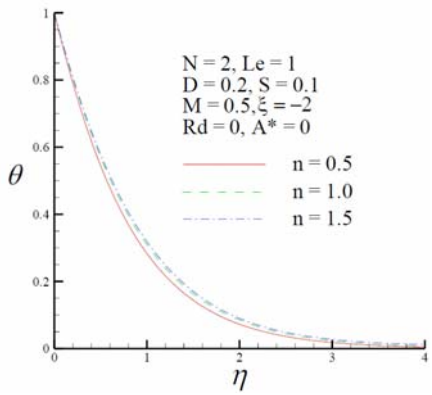

(a)

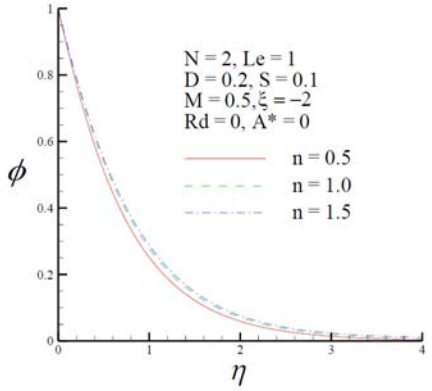

(b)

Figure 4. (a) The dimensionless temperature profile and (b) the dimensionless concentration profile for three values of the non-Newtonian fluid *n*.

Figure 4 portrays the dimensionless temperature and concentration profiles for three values of the non-Newtonian fluid n (n = 0.5, 1.0 and 1.5) with $N = 2$, $Le = 1$, $D = 0.2$, $S = 0.1$, $M = 0.5$, $\xi = -2$, $R_d = 0$, $A^* = 0$, respectively. It is obviously found that the dimensionless temperature profiles $\theta(\xi, \eta)$ and the dimensionless concentration profiles $\phi(\xi, \eta)$ decrease slightly with decreasing the non-Newtonian fluid n, thus

decreasing the thermal and concentration boundary layer thicknesses. The analysis has shown that the dimensionless temperature and concentration profiles are slightly influenced by non-Newtonian fluid.

Table 7. The values of $Nu_x/Ra_x^{1/2n}$ and $Sh_x/Ra_x^{1/2n}$ for various values of n with $N = 2$, $Le = 1$, $D = 0.2$, $S = 0.1$, $M = 0.5$, $\xi = -2.0$, $R_d = 0$ and $A^* = 0$

n	$Nu_x/Ra_x^{1/2n}$	$Sh_x/Ra_x^{1/2n}$
0.5	1.1365	1.2585
0.8	1.0821	1.1974
1.0	1.0621	1.1745
1.5	1.0367	1.1449
2.0	1.0226	1.1277

Table 7 lists the values of local Nusselt number $Nu_x/Ra_x^{1/2n}$ and the local Sherwood number $Sh_x/Ra_x^{1/2n}$ for various values of the non-Newtonian fluid n with $N = 2$, $Le = 1$, $D = 0.2$, $S = 0.1$, $M = 0.5$, $\xi = -2$, $R_d = 0$ and $A^* = 0$. It is also found that reducing the non-Newtonian fluid n enhances both the local Nusselt number and the local Sherwood number. This is because reducing the non-Newtonian fluid n tends to enhance the velocity of the flow and increase the dimensionless surface temperature and concentration gradients, as shown in Figure 4. Therefore, pseudoplastic fluids $(n = 0.5)$ are superior to the dilatant fluids $(n = 1.5)$ from the viewpoint of the heat and mass transfer rates by natural convection from a vertical plate embedded in a porous medium saturated with non-Newtonian power-law fluids.

Figure 5 presents the dimensionless temperature and concentration profiles for three values of the thermal radiation parameter R_d ($R_d = 0$, 2 and 5) with $N = 2$, $Le = 1$, $D = 0.2$, $S = 0.1$, $n = 1.5$, $M = 0$, $A^* = 1$, $\xi = -1$, respectively. Figure 5(a) shows that, as the value of thermal radiation parameter R_d increases, the radiation absorption in the boundary

layer increases, which increases the sizes of the dimensionless temperature profiles, but the dimensionless surface temperature gradient $-\theta'(\xi, 0)$ becomes small. However, Figure 5(b) shows that increasing the thermal radiation parameter R_d, increases the dimensionless surface concentration gradient $-\phi'(\xi, 0)$.

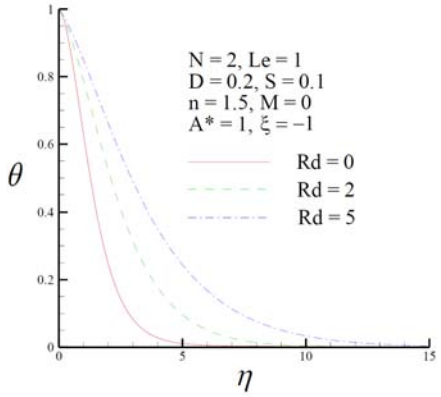

(a)

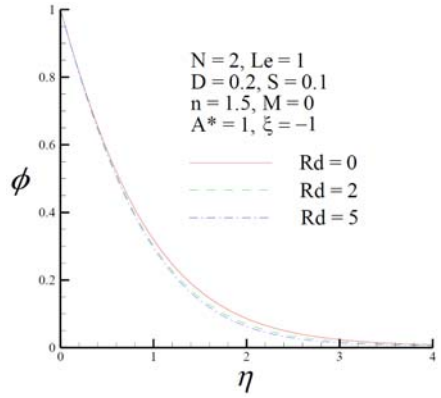

(b)

Figure 5. (a) The dimensionless temperature profile and (b) the dimensionless concentration profile for three values of the thermal radiation parameter R_d.

Table 8. The values of $Nu_x/Ra_x^{1/2n}$ and $Sh_x/Ra_x^{1/2n}$ for various values of ξ with $N = 2,\ Le = 1,\ D = 0.2,\ S = 0.1,\ n = 1.5,\ M = 0,\ A^* = 1,\ \xi = -1$

R_d	$Nu_x/Ra_x^{1/2n}$	$Sh_x/Ra_x^{1/2n}$
0	0.0608	0.9881
2	0.4281	0.9902
5	0.7899	0.9939
8	1.0776	0.9957
10	1.2493	0.9965

Table 8 lists the values of local Nusselt number $Nu_x/Ra_x^{1/2n}$ and the local Sherwood number $Sh_x/Ra_x^{1/2n}$ for various values of R_d with $N = 2,\ Le = 1,\ D = 0.2,\ S = 0.1,\ n = 1.5,\ M = 0,\ A^* = 1,\ \xi = -1$. It is seen that the value of the local Nusselt number increases with increasing the value of R_d. In the pure convection heat transfer, the local Nusselt number is only proportional to the dimensionless surface temperature gradient $-\theta'(\xi, 0)$. For the case of large R_d (radiation effect becomes pronounced), although $-\theta'(\xi, 0)$ is low as shown in Figure 5, the local Nusselt number is still large. This is because the local Nusselt number is found to be more sensitive to R_d than $-\theta'(\xi, 0)$, as revealed in equation (30). However, enhancing the thermal radiation parameter R_d increases slightly the local Sherwood number. This is because enhancing the thermal radiation parameter R_d increases the dimensionless surface concentration gradient $-\phi'(\xi, 0)$. With the aid of equation (31), the greater the dimensionless surface concentration gradient, the larger the local Sherwood number.

The effect of the internal heat generation coefficient A^* ($A^* = 0.0,\ 0.5$ and 1.0) on the dimensionless temperature profile and the dimensionless concentration profile with $N = 2,\ Le = 1,\ D = 0.2,\ S = 0.1,\ n = 1.5,\ M = 0,\ R_d = 1$ and $\xi = -1$, is plotted in Figure 6, respectively. It is observed that the increase of the internal heat generation coefficient A^* leads to a tendency to decrease the dimensionless wall temperature gradient

$-\theta'(\xi, 0)$ but increase the dimensionless wall concentration gradient $-\phi'(\xi, 0)$.

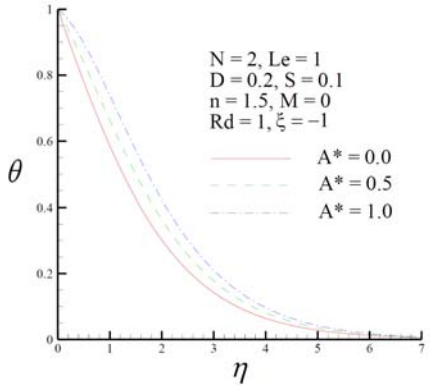

(a)

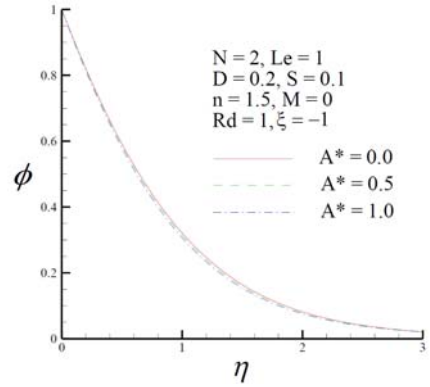

(b)

Figure 6. (a) The dimensionless temperature profile and (b) the dimensionless concentration profile for three values of the internal heat generation coefficient A^*.

Table 9 lists the values of local Nusselt number $Nu_x / Ra_x^{1/2n}$ and the local Sherwood number $Sh_x / Ra_x^{1/2n}$ for various values of the internal heat generation coefficient A^* with $N = 2$, $Le = 1$, $D = 0.2$, $S = 0.1$, $n = 1.5$, $M = 0$, $R_d = 1$ and $\xi = -1$. In general, it has been found that enhancing

the internal heat generation coefficient A^* reduces the local Nusselt number and enhances slightly the local Sherwood number. This is due to the fact that enhancing the internal heat generation coefficient A^* tends to decreases the dimensionless surface temperature gradients and increases the dimensionless surface concentration gradients, as shown in Figure 6, thus lowering the local Nusselt number and highering the local Sherwood number.

Table 9. The values of $Nu_x/Ra_x^{1/2n}$ and $Sh_x/Ra_x^{1/2n}$ for various values of ξ with $N = 2,\ Le = 1,\ D = 0.2,\ S = 0.1,\ n = 1.5,\ M = 0,\ R_d = 1,\ \xi = -1$

A^*	$Nu_x/Ra_x^{1/2n}$	$Sh_x/Ra_x^{1/2n}$
0.0	1.0729	0.9457
0.25	0.8707	0.9565
0.50	0.6695	0.9672
0.75	0.4694	0.9777
1.0	0.2701	0.9881

5. Conclusions

A two-dimensional, laminar boundary layer analysis is presented to study the influence of uniform blowing/suction on the MHD-natural convection of non-Newtonian fluids over a vertical plate in porous media with internal heat generation, thermal radiation and Soret/Dufour effects. After the coordinate transformation, the transformed governing equations are solved by Keller box method (KBM). Comparisons with previously published works show excellent agreement. Numerical solutions are obtained for different values of the magnetic field parameter *M*, the power-law index of the non-Newtonian fluid *n*, the blowing/suction parameter ξ, the internal heat generation coefficient A^* and the thermal radiation parameter R_d. Results show that increasing the magnetic field parameter *M* or the power-law index of non-Newtonian fluid *n* tends to reduce both the local Nusselt number and the local Sherwood number. Otherwise, when the thermal radiation parameter R_d increases, both the local Nusselt number and the local Sherwood number increase. In addition, increasing the internal heat generation coefficient A^*

tends to reduce the local Nusselt number and enhances the local Sherwood number. In general, for the case of suction, both the local Nusselt number and the local Sherwood number increase. This trend is reversed for blowing of fluid.

References

[1] D. A. Nield and A. Bejan, Convection in Porous Media, Springer-Verlag, New York, 2013.

[2] M. Anghel, H. S. Takhar and I. Pop, Dufour and Soret effects on free convection boundary-layer flow over a vertical surface embedded in a porous medium, Stud. Univ. Babes-Bolyai Math. 45 (2000), 11-23.

[3] C. Y. Cheng, Double diffusion from a vertical wavy surface in a porous medium saturated with a non-Newtonian fluid, Int. Commun. Heat Mass Transf. 34 (2007), 285-294.

[4] A. Postelnicu, Heat and mass transfer by natural convection at a stagnation point in a porous medium considering Soret and Dufour effects, Heat and Mass Transfer 46 (2010), 831-840.

[5] C. Y. Cheng, Soret and Dufour effects on free convection heat and mass transfer from an arbitrarily inclined plate in a porous medium with constant wall temperature and concentration, Int. Commun. Heat Mass Transf. 39 (2012), 72-77.

[6] A. V. Shenoy, Non-Newtonian fluid heat transfer in porous media, Advances in Heat Transfer 24 (1994), 102-184.

[7] H. T. Chen and C. K. Chen, Natural convection of non-Newtonian fluids along a vertical plate embedded in a porous medium, ASME J. Heat Transf. 110 (1988), 257-260.

[8] R. S. R. Gorla and M. Kumari, Nonsimilar solutions for free convection in non-Newtonian fluids along a vertical plate in a porous medium, Internat. J. Numer. Methods Heat Fluid Flow 9 (1999), 847-859.

[9] C. Y. Cheng, Natural convection heat and mass transfer of non-Newtonian power law fluids with yield stress in porous media from a vertical plate with variable wall heat and mass fluxes, Int. Commun. Heat Mass Transf. 33 (2006), 1156-1164.

[10] A. Mahdy and F. M. Hady, Effect of thermophoretic particle deposition in non-Newtonian free convection flow over a vertical plate with magnetic field effect, Journal of Non-Newtonian Fluid Mechanics 161 (2009), 37-41.

[11] J. C. Crepeau and R. Clarksean, Similarity solutions of natural convection with internal heat generation, J. Heat Transf. 119 (1997), 183-185.

[12] A. Postelnicu and I. Pop, Similarity solutions of free convection boundary layers over vertical and horizontal surfaces in porous media with internal heat generation, Int. Commun. Heat Mass Transf. 26 (1999), 1183-1191.

[13] T. Grosan and I. Pop, Free convection over vertical flat plate with a variable wall temperature and internal heat generation in a porous medium saturated with a non-Newtonian fluid, Technische Mechanik 21 (2001), 313-318.

[14] E. A. Mohamed, The effect of lateral mass flux on the natural convection boundary layers induced by a heated vertical plate embedded in a saturated porous medium with internal heat generation, International Journal of Thermal Sciences 46 (2007), 157-163.

[15] M. A. A. Mahmoud, Radiation effect on free convection of a non-Newtonian fluid over a vertical cone embedded in a porous medium with heat generation, J. Appl. Mech. Tech. Phys. 53 (2012), 743-750.

[16] K. A. Yih and C. J. Huang, Effect of internal heat generation on free convection heat and mass transfer of non-Newtonian fluids flow over a vertical plate in porous media: VWT/VWC, Journal of Aeronautics, Astronautics and Aviation 47 (2015), 115-122.

[17] A. Raptis, Radiation and free convection flow through a porous medium, Int. Commun. Heat Mass Transf. 25 (1998), 289-295.

[18] A. A. Mohammadien and M. F. El-Amin, Thermal dispersion-radiation effects on non-Darcy natural convection in a fluid saturated porous medium, Transport in Porous Media 40 (2000), 153-163.

[19] M. A. El-Hakiem and M. F. El-Amin, Thermal radiation effect on non-Darcy natural convection with lateral mass transfer, Heat and Mass Transfer 37 (2001), 161-165.

[20] M. A. Seddeek, Thermal radiation and buoyancy effects on MHD free convective heat generating flow over an accelerating permeable surface with temperature-dependent viscosity, Canadian Journal of Physics 79 (2001), 725-732.

[21] B. C. Tai and M. I. Char, Soret and Dufour effects on free convection flow of non-Newtonian fluids along a vertical plate embedded in a porous medium with thermal radiation, Int. Commun. Heat Mass Transf. 37 (2010), 480-483.

[22] M. Sheikholeslami, D. D. Ganji, M. Y. Javed and R. Ellahi, Effect of thermal radiation on magnetohydrodynamics nanofluid flow and heat transfer by means of two phase model, Journal of Magnetism and Magnetic Materials 374 (2015), 36-43.

[23] C. Y. Cheng, Effect of magnetic field on heat and mass transfer by natural convection from vertical surfaces in porous media - an integral approach, Int. Commun. Heat Mass Transf. 26 (1999), 935-943.

[24] A. Postelnicu, Influence of a magnetic field on heat and mass transfer by natural convection from vertical surfaces in porous media considering Soret and Dufour effects, Int. J. Heat Mass Transf. 47 (2004), 1467-1472.

[25] C. Y. Cheng, An integral approach for hydromagnetic natural convection heat and mass transfer from vertical surfaces with power-law variation in wall temperature and concentration in porous media, Int. Commun. Heat Mass Transf. 32 (2005), 204-213.

[26] M. K. Partha, P. V. S. N. Murthy and G. P. Raja Sekhar, Soret and Dufour effects in a non-Darcy porous medium, ASME J. Heat Transf. 128 (2006), 605-610.

[27] A. Y. Bakier and M. A. Mansour, Combined of magnetic field and thermophoresis particle deposition in free convection boundary layer from a vertical flat plate embedded in a porous medium, Thermal Science 11 (2007), 65-74.

[28] A. M. Rashad, Influence of radiation on MHD free convection from a vertical flat plate embedded in porous media with thermophoretic deposition of particles, Commun. Nonlinear Sci. Numer. Simul. 13 (2008), 2213-2222.

[29] A. J. Chamkha and A. Ben-Nakhi, MHD mixed convection-radiation interaction along a permeable surface immersed in a porous medium in the presence of Soret and Dufour's effects, Heat and Mass Transfer 44 (2008), 846-856.

[30] A. Mahdy, A. J. Chamkha and Y. Baba, Double-diffusive convection with variable viscosity from a vertical truncated cone in porous media in the presence of magnetic field and radiation effects, Comput. Math. Appl. 59 (2010), 3867-3878.

[31] V. R. Prasad, B. Vasu and O. A. Bég, Thermo-diffusion and diffusion-thermo effects on MHD free convection flow past a vertical porous plate embedded in a non-Darcian porous medium, Chemical Engineering Journal 173 (2011), 598-606.

[32] C. Y. Hsiao, W. J. Chang, M. I. Char and B. C. Tai, Influence of thermophoretic particle deposition on MHD free convection flow of non-Newtonian fluids from a vertical plate embedded in porous media considering Soret and Dufour effects, Appl. Math. Comput. 244 (2014), 390-397.

[33] R. V. Christopher and S. Middleman, Power-law flow through a packed tube, Industry and Engineering Chemistry Fundamentals 4 (1965), 424-426.

[34] R. V. Dharmadhirkari and D. D. Kale, Flow of non-Newtonian fluids through porous media, Chemical Engineering Science 40 (1985), 527-529.

[35] T. Cebeci and P. Bradshaw, Physical and Computational Aspects of Convective Heat Transfer, Springer-Verlag, New York, 1984.